TD-DFT Description of Photoabsorption and Electron Transfer in a Covalently Bonded Porphyrin−Fullerene Dyad

Oana Cramariuc,*,†,‡ Terttu I. Hukka,‡ Tapio T. Rantala,† and Helge Lemmetyinen‡

Institute of Physics, Tampere University of Technology, P.O. Box 692, FIN-33101, Tampere, Finland, and Institute of Materials Chemistry, Tampere University of Technology, P.O. Box 541, FIN-33101, Tampere, Finland

Structure, photoabsorption, and excited states of a covalently bonded porphyrin−fullerene dyad $H_2P−O34−C_{60}$ are studied using DFT and TD-DFT approaches. Charge transfer from the donor (porphyrin) to the acceptor (fullerene) and the excited-state geometrical relaxation are of special interest. An analysis of differences in the description of these delicate phenomena due to the different exchange-correlation functionals is presented. We compare the results given by LDA, GGA, and hybrid functionals (i.e., SVWN, PBE, B3LYP, and PBE0). The ground-state center-to-center (cc) equilibrium distance between the donor and the acceptor moieties is 6.3, 7.1, and 7.9 Å with SVWN, PBE, and B3LYP, respectively. The associated charge transfer of 0.15, 0.11, and 0.09 electrons is shown to depend on this distance but not directly on the functional itself. The same trend is seen in the HOMO−LUMO difference results, and further, in the lowest excitation energies, except for the hybrid functional calculations that yield the largest HOMO−LUMO gap and the highest energy for the lowest electronic excitation. The hybrid functionals were not found practical for excited-state conformational relaxation with the present computing resources. With LDA, the relaxation increases the cc distance by about 0.2 Å, which is associated with a 0.14 eV decrease in energy. As compared to the ground-state dipole moment of about 4 D, the relaxed excited-state charge-transfer complex dipole moment turns out to become about 20 D. A local excitation of the porphyrin donor is considered, as well, and based on all these results, the nature and interpretation of the photoinduced electron-transfer process is discussed.

1. Introduction

Owing to the importance and complexity of natural photosynthesis, substantial efforts have over the past decades been directed to mimicking the photoinduced electron transfer (ET) and charge separation taking place in natural photosynthetic reaction centers. The ultimate goals are to understand at the quantum chemical level the steps and mechanisms involved in photosynthesis at the molecular level. An important approach toward mimicking the processes involved in photosynthesis consists of building molecular ensembles (polyads: dyads, triads, etc.) by covalently linking electron donor and acceptor molecules. In this case, the linker that is responsible for partially or totally restricting the distance and relative orientation between the donor and the acceptor[1] can be considered as a functional substitute of the protein framework existing in natural photosynthetic reaction centers.

Porphyrins and fullerenes are examples of donor and acceptor molecules used to mimic the photosynthetic processes. They have been extensively used for building molecular polyads that demonstrate photoinduced electron transfer.[2−9] In particular, the porphyrin−fullerene (P−C_{60}) dyad $H_2P−O34−C_{60}$ illustrated in Figure 1 has aided in better understanding of the ET pathways following photoexcitation.[3,10] In both nonpolar and polar solvents, the photophysical behavior of $H_2P−O34−C_{60}$ can be explained in terms of a simultaneous presence of two extreme conformations of the dyad: a predominant folded one and an
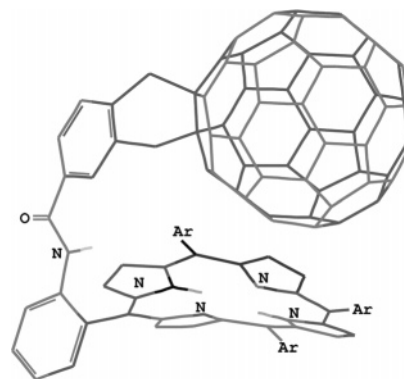

Figure 1. Molecular structure of $H_2P−O34−C_{60}$ in which Ar stands for the aromatic 3,5-(t-butyl)$_2C_6H_3$. Single and double bonds are shown explicitly only for the linker, and the hydrogen atoms have been omitted except for the hydrogens attached to the nitrogen atoms.

extended one.[3,10] In the folded conformation, the porphyrin and fullerene molecules are in close proximity as opposed to the extended conformation that is characterized by a large P−C_{60} distance. Our previously reported molecular dynamics (MD) simulations of $H_2P−O34−C_{60}$ also predict the existence of two conformations.[11] It is, however, important to notice that the molecular chain linking the fullerene and porphyrin molecules is quite flexible, allowing other conformations, including folded ones with several different P−C_{60} distances, to also be accessible at relatively small energy expenses. This is well-demonstrated by our previous MD simulations, which yield relatively wide P−C_{60} distance distributions.[11]

* Corresponding author. E-mail: oana.cramariuc@tut.fi.
† Institute of Physics.
‡ Institute of Materials Chemistry.

Porphyrin−Fullerene Photoabsorption/Electron Transfer

J. Phys. Chem. A, Vol. 110, No. 45, 2006 **12471**

In the case of the folded conformation, considerable ground-state interactions between the porphyrin and the fullerene molecules is seen in the absorption spectrum of $H_2P-O34-C_{60}$.[3,10] The spectrum of the $H_2P-O34-C_{60}$ dyad is broader, lower in intensity, and shifted to the red in the Soret band region as compared to the sum spectrum of H_2P-O34 and C_{60}. It also exhibits in the near-infrared (NIR) region an additional broad weak band that corresponds to the absorption of a charge-transfer (CT) complex formed at the ground state of the dyad. The CT complex is a result of the redistribution of the electron density due to the interaction of porphyrin and fullerene.[3,10,12,13] Investigations involving the direct excitation of the ground-state CT complex (g-CTC) to its Franck−Condon (F−C) state and the subsequent conformational relaxation of the excited state to the minimum of its potential energy surface (PES) would make it possible to directly observe the formation of the excited CT complex (ex-CTC) state.[12] The ex-CT complex is also called exciplex because there is no formal difference between an ex-CT complex and an exciplex.[13] The main difference when distinguishing between an exciplex and an ex-CT complex relates to their formation. Exciplexes have no ground-state counterparts and exist only in the excited states through the interaction of an excited donor or an acceptor with a ground-state acceptor or donor, respectively. On the other hand, ex-CTC has a ground-state counterpart (i.e. g-CTC), and thus, it can be formed by a direct excitation of g-CTC. However, direct spectroscopic investigations of ex-CTC pose several difficulties including a low absorption of g-CTC.[12]

Generally, the experimental measurements elucidating the dynamics and excited-state intermediates after the photoexcitation of the porphyrin moiety of $H_2P-O34-C_{60}$ use 410 nm as an excitation wavelength. Following the photoexcitation of $H_2P-O34-C_{60}$, three intermediate excited states have been identified prior to the relaxation to the ground state: (a) the locally excited singlet porphyrin state $(H_2P-O34)^{1S}-C_{60}$, (b) ex-CTC, and (c) the charge-separated (CSS) state $(H_2P-O34)^+-C_{60}^-$, which is identified in polar solvents only.[3,10] The (a) and (c) excited states together with the locally excited singlet and triplet states of fullerene are commonly identified as intermediate states following the photoexcitation of various $P-C_{60}$ dyads described in the literature.[3,10,14−17] In addition, studies carried out during the recent years have shed light on the role of the intramolecular ex-CTC/exciplex as an important intermediate step in the photophysics of $P-C_{60}$ (and related) systems.[4−9]

Presently, investigations broadly focus on the performance of quantum chemical methodologies for calculating excited-state properties such as excited-state equilibrium geometries and spectral parameters (e.g., absorption and emission maxima). In addition, also the porphyrin−fullerene interaction producing g-CTC represents an important and demanding testing ground for the DFT functionals, due to the delicate balance between the dispersion, polarization, and CT contributions in the description of these complexes.[18,19]

In the case of large molecules, the time-dependent density functional theory (TD-DFT) based method has been proven to be a practical alternative to conventional highly correlated wave function methods employing large active spaces and thus being tedious and time-consuming. The reliability of the TD-DFT approach in obtaining accurate predictions of excitation energies and oscillator strengths is well-documented for a wide range of molecules (i.e., from small[20−24] to large ones),[25,26] including higher fullerenes,[27] free-base porphyrin,[28] and transition-metal tetrapyrroles.[29] However, theoretical investigations of long-range

CT excited states represent a challenging task even for highly correlated wave function theory methods. In addition, it has been claimed that in such cases, TD-DFT might not offer a general solution.[30−32] It has also been shown that the description of long-range CT excited states depends on the chosen exchange-correlation functional.[30,33] Thus, specific tests with various functional approximations are essential in evaluating the performance and accuracy of TD-DFT and in predicting the electron-transfer properties of molecules with a long distance between the donor and the acceptor, in particular. Moreover, while tests on small and simple molecules are readily available, calculations on large molecules and molecular complexes that are computationally highly demanding prove to be a challenging task.

In this quantum chemical study, we focus on the computational investigation of a folded conformer of $H_2P-O34-C_{60}$. We present DFT calculations on the ground-state structure and the electronic properties of $H_2P-O34-C_{60}$. In addition, we present TD-DFT calculations on the excited-state properties of $H_2P-O34-C_{60}$. The goal is to assess the performance and accuracy of DFT and TD-DFT when applied to the following properties of $H_2P-O34-C_{60}$: (a) the interaction of porphyrin and fullerene in the ground state of the dyad and the CT character of the ground state, (b) the excitation energies of the dyad and especially the energy corresponding to the excitation of g-CTC, (c) the relaxation of the Franck−Condon state of the g-CT complex to the ex-CT complex, and (d) the energy and structure of the ex-CT complex.

2. Computational Methods

Both the local-density (LDA) and the generalized-gradient (GGA) approximations to the exchange-correlation energy functional are used. In particular, the Slater−Vosko−Wilk−Nusair (SVWN) functional[34,35] is employed in the LDA calculations and the Perdew−Burke−Ernzerhof (PBE) functional[36−39] in the GGA calculations. In addition, two hybrid functionals are used for those calculations for which the increase in computational time did not prove prohibitive. In particular, Becke's three parameter hybrid functional with the Lee−Yang−Parr correlation functional (B3LYP)[35−37,40,41] and the PBE0[42] are tested. It may be worthwhile to point out that in general, LDA and GGA functionals present a more systematic behavior, although hybrid functionals may match better with experiments.

The basis set used throughout the calculations is the Karlsruhe split-valence basis set augmented with polarization functions (SVP).[43,44] The SVP basis set consists of two basis functions for H (4s)/[2s], six basis functions for C (7s4p1d)/[3s2p1d], and six basis functions for N (7s4p1d)/[3s2p1d]. The terms in parentheses and square brackets represent the numbers of primitive functions and of contracted basis functions of each type, respectively. The resolution of identity approach (RI) is used in the LDA and GGA calculations to reduce the computational effort.[45] All DFT and TD-DFT calculations are performed with the Turbomole software package.[46] The TD-DFT excited-state geometry optimizations are carried out as described in ref 52 and implemented in the Turbomole software package.

3. Results

3.1. Ground-State Geometry. Some structural characteristics of the molecular geometry of $H_2P-O34-C_{60}$ optimized at the DFT level using the SVWN, PBE, and B3LYP functionals are presented in Table 1. The results of the DFT/PBE and semiempirical (SE) optimizations have been reported in our previous paper[11] and are shown for comparison in Table 1. The

12472 *J. Phys. Chem. A, Vol. 110, No. 45, 2006*

Cramariuc et al.

TABLE 1: Ground-State Porphyrin−Fullerene Center-to-Center (cc) Distances and rms Deviations of the Porphyrin Ring from Least-Squares Plane Given in Ångströms (Å) as Obtained from Different Geometry Optimizations[a]

	DFT			SE	
	SVWN	PBE	B3LYP	AM1	PM3
cc distance (Å)	6.3	7.1	7.9	9.0	8.2
rms deviation (Å)	0.15	0.10	0.09	0.05	0.05

[a] Diameter of fullerene is approximately 7 Å. The SE results have been taken from ref 11.

first row of Table 1 contains the center-to-center (cc) distance of each optimized structure. The cc distance represents the distance between the center of fullerene and the center of the porphyrin ring. The distance is mainly determined by the interaction between the porphyrin and the fullerene moieties. The interaction includes the CT interaction, as pointed out previously.[18,19] The second row of Table 1 represents the root-mean-square (rms) deviation from the least-squares plane calculated for the 24 atoms of the porphyrin ring. The rms deviation is a measure of the nonplanarity of the porphyrin ring, while the positioning of the porphyrin ring atoms above or below the least-squares plane forms the basis of classifying nonplanar porphyrins.[47] The prophyrin ring is in all cases in a ruffled conformation.[47]

Three different functionals used yielded cc distances that differ by more than 1.5 Å. The smallest and largest cc distances were obtained from the SVWN and B3LYP calculations, respectively. On the basis of the calculated data given in Table 1, the cc distance decreases in the following order: SE > DFT/B3LYP > DFT/PBE > DFT/SVWN. An opposite variation is observed for the nonplanarity of the porphyrin ring. The smallest cc distance may relate to the overestimation of binding in the LDA approach. However, as there is no experimental data such as X-ray diffraction data for comparison, further investigations such as evaluation of the spectroscopic properties of the LDA, GGA, and hybrid functional structures are needed.

The cc distance is known to influence the extent of CT between the donor and the acceptor in the ground state of the dyad. The electric dipole moment is used as a measure of the amount of CT. The electric dipole moments of the DFT optimized dyad structures with different cc distances (see Table 2) are obtained from single-point (SP) calculations using the SVWN, PW91, B3LYP, and PBE0 functionals for each of the DFT structures referred to in Table 1. In addition, the calculated dipole moments are given as percentages of maximum dipole moments arising from the transfer of one electron from the center of the porphyrin to the center of the fullerene. Regardless of the functional, the dipole moment increases with a decreasing cc distance, indicating an increase of the charges on the fullerene

and porphyrin moieties. Moreover, while the values (see Table 2) of the calculated dipole moments vary in the range of 3.4−4.4 D, the orientations of the dipole moments are always along the axis connecting the center of the porphyrin to the center of the fullerene. These results support the CT character of the dyad in the ground state, which increases when the cc distance between the donor and the acceptor decreases. The values obtained for the electric dipole moment of $H_2P-O34-C_{60}$ are close to the one reported by Parusel[48] for a different porphyrin−fullerene dyad, and in addition, are approximately 4 times larger than the dipole moment reported for a linked fullerene−oligothiophene dyad.[49]

3.2. Electronic Structure. The energies of some of the highest and lowest occupied molecular orbitals of $H_2P-O34-C_{60}$ are given in Table 3. The HOMO and LUMO wave functions are presented as isoamplitude surfaces in Figure 2. The same isoamplitude surface value is used for all plots, thus allowing a facile comparison between the localization and the delocalization of the same orbital.

To evaluate the influence of the functional and the cc distance on the delocalization and on the energies of molecular orbitals, single-point calculations using the SVWN, PW91, B3LYP, and PBE0 functionals were carried out for each of the DFT structures referred to in Table 1. The single-point results obtained with different functionals for the same cc distance display, as expected, HOMO−LUMO energy gaps increased by at least 1 eV for hybrid functionals as compared to the LDA and GGA functionals. The largest value is obtained from PBE0 calculations. The increase of the HOMO−LUMO gap is mainly due to the LUMO orbital energy that is shifted up, except for the PBE0 functional that shifts the energies of both HOMO and LUMO even when compared to B3LYP. For the same functional, the molecular orbital energies present significantly larger variations when the cc distance decreases from 7.1 to 6.3 Å than when decreasing from 7.9 to 7.1 Å. It is the LUMO orbital energy that the structural changes always influence the most. The isoamplitude surfaces of the HOMO and LUMO begin to be delocalized over both the porphyrin and the fullerene moieties as the cc distance decreases (see Figure 2).

3.3. Optical Absorption Properties. The TD-DFT method is used to evaluate the excitation energies and oscillator strengths of the electronic excitations of $H_2P-O34-C_{60}$ in the visible and near-IR region of the spectrum. The energies and the oscillator strengths of the electronic transition to the lowest excited state (i.e., the energy corresponding to a direct excitation of g-CTC) obtained by TD-DFT with different functionals are given in Table 4. In addition, the experimental absorption energy corresponding to the experimental absorption maximum is also given in Table 4. Because no experimental gas-phase absorption spectrum is available for $H_2P-O34-C_{60}$, the liquid-phase data with benzene as a solvent is given.[3,10]

TABLE 2: Ground-State Electric Dipole Moments Given in Debyes,[a] Obtained from Single-Point Calculations Using the SVWN, PW91, B3LYP, and PBE0 Functionals for the Geometries Defined in Table 1[b]

functional for SP calculations/ cc distance of optimized structures	6.3 (SVWN optimization)	7.1 (PBE optimization)	7.9 (B3LYP optimization)	
SVWN	4.4	3.8	3.5	dipole
	15	11	9	%
PBE	4.3	3.7	3.4	dipole
	14	11	9	%
B3LYP	4.2	3.6	3.4	dipole
	14	11	9	%
PBE0	4.3	3.7	3.5	dipole
	14	11	9	%

[a] 1 D = 3.33×10^{-30} cm. [b] Dipole moments are also given as percentages of the dipole moment related to the transfer of one electron.

TABLE 3: Calculated Orbital Eigenvalue Energies (eV) of the Frontier Molecular Orbitals for Geometries Defined in Table 1[a]

functional for optimization/ functional for SP calculations	SVWN (6.3 Å)	PBE (7.1 Å)	B3LYP (7.9 Å)	
SVWN	1.04	0.87	0.87	LUMO + 1
	0.97	0.81	0.80	LUMO
	0.00 (−5.02)	0.00 (−4.99)	0.00 (−4.98)	HOMO
	−0.39	−0.39	−0.38	HOMO − 1
PBE	1.06	0.91	0.89	LUMO + 1
	0.99	0.85	0.83	LUMO
	0.00 (−4.80)	0.00 (−4.78)	0.00 (−4.76)	HOMO
	−0.39	−0.39	−0.37	HOMO − 1
B3LYP	2.02	1.88	1.89	LUMO + 1
	1.93	1.80	1.80	LUMO
	0.00 (−5.17)	0.00 (−5.16)	0.00 (−5.15)	HOMO
	−0.39	−0.34	−0.32	HOMO − 1
PBE0	2.22	2.09	2.10	LUMO + 1
	2.13	2.00	2.01	LUMO
	0.00 (−5.48)	0.00 (−5.48)	0.00 (−5.47)	HOMO
	−0.40	−0.33	−0.31	HOMO − 1

[a] HOMO energy is used as a reference, and the absolute values are given in parentheses.
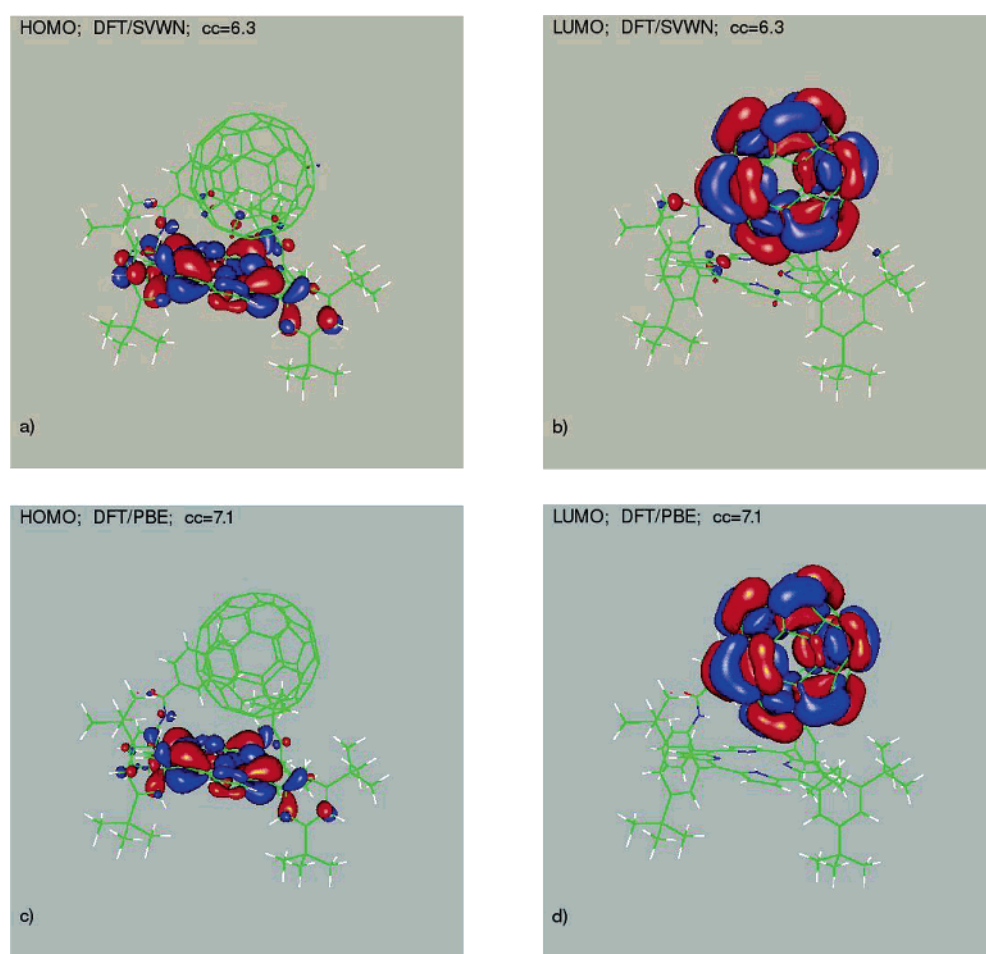

Figure 2. HOMO and LUMO presented as isoamplitude surfaces for structures having different cc distances. The cc distances are given in angstroms. Relative phases of the wave function are indicated by regions of different colors.

It can be seen by comparing the results presented in Table 4 that the largest values for the excitation energies are obtained with the hybrid functionals. In particular, the energy of 1.61 eV for the first excitation obtained from the PBE0 calculations on the SVWN optimized geometry has the largest value and compares best with the experimental absorption maximum of ca. 1.7 eV. The difference between the excitation energies calculated with the same hybrid functionals for different optimized structures is probably due to the differences in cc distances in these structures. However, there is no consistent dependence of the excitation energy on the cc distance (i.e.,

the distance increases as SVWN < PBE < B3LYP, while the excitation energy decreases as SVWN > B3LYP > PBE. Thus, other factors, such as the overall geometrical characteristics of the B3LYP, SVWN, and PBE optimized structures, are probably responsible for the differences in excitation energies.

The one-electron transition from HOMO to LUMO contributes to the first singlet electronic excitation of the dyad and depends on the structure and functional with a weight varying from 97.6 to 100%. Calculations with the SVWN structure, which has the shortest cc distance, yield the smallest contributions of the HOMO−LUMO transitions, independent of whether

TABLE 4: TD-DFT Transition Energies and Oscillator Strengths of First Singlet Electronic Excitation of the Dyad (eV)[a]

functional for SP calculations/ functional for optimization	SVWN (6.3 Å)	PBE (7.1 Å)	B3LYP (7.9 Å)	
SVWN	0.99	0.81	0.80	transition energy
	5.9	1.1	0.14×10^{-1}	oscillator strength $\times 10^{-3}$
PBE	1.01	0.84	0.83	transition energy
	5.8	1.1	0.13×10^{-1}	oscillator strength $\times 10^{-3}$
B3LYP	1.52	1.43	1.46	transition energy
	9.0	1.0	0.74×10^{-2}	oscillator strength $\times 10^{-3}$
PBE0	1.61	1.54	1.58	transition energy
	9.6	1.1	0.82×10^{-2}	oscillator strength $\times 10^{-3}$

[a] Experimental transition energy measured in benzene solution is ∼1.7 eV.

the LDA, GGA, or hybrid functional is used. On the other hand, the TD-DFT calculations on the PBE and B3LYP optimized structures that have an intermediate and a long cc distances, respectively, yield contributions of at least 99%, independent of the functional used. Thus, we can conclude that the contribution of the HOMO−LUMO one-electron transition is mainly influenced by the distance between porphyrin and fullerene (i.e., by the amount of their interaction).

As pointed out previously, the electronic transition to the first excited state corresponds basically to a one-electron transition from HOMO to LUMO. Thus, its energy is mainly influenced by the HOMO−LUMO orbital energy difference, which enters the TD-DFT formalism as a first approximation to the transition energy. While both LDA and GGA functionals underestimate the HOMO−LUMO energy gap, this is significantly corrected by the use of hybrid functionals. It is therefore not surprising that hybrid functionals yield energies that are the largest and closest to the experimental energy value for the first electronic transition.

The calculated oscillator strengths are ca. 0.01−0.001, except in the case of the TD-DFT calculation on the B3LYP optimized structure, which is 3−4 orders of magnitude smaller (see Table 4). Because the single-point calculations with the SVWN and PBE functionals on the B3LYP optimized structure yield oscillator strengths, which are close in orders of magnitude to the one yielded by B3LYP, we expect that the low oscillator strength results mostly from a large cc distance in the B3LYP optimized structure.

Calculations of the electronic excitations with energies larger than the first excited singlet state yield several electronic excitations that involve transitions from orbitals localized on porphyrin or fullerene to orbitals localized on fullerene. An excitation that corresponds to the formation of a locally excited singlet porphyrin state $(H_2P-O34)^{1S}-C_{60}$ follows, and it involves mainly contributions from transitions between orbitals localized on porphyrin. The energy of the excitation leading to the first locally excited singlet porphyrin state $(H_2P-O34)^{1S}-C_{60}$ seems to depend little on the structural characteristics, such as the cc distance, and on the functional. The calculated excitation energy values range from 1.9 to 2.0 eV, as compared to the experimental value of 1.89 eV. However, the number of electronic excitations calculated between the excitation of g-CTC and the first locally excited singlet porphyrin state $(H_2P-O34)^{1S}-C_{60}$ depends largely on the functional that is used. The B3LYP functional yields the smallest number of excitations. It is possible that the use of PBE0 for higher energy calculations would further decrease the number of excitations between the excitation of g-CTC and the first locally excited singlet porphyrin state $(H_2P-O34)^{1S}-C_{60}$. Unfortunately, these calculations proved to be computationally too expensive. The present results are similar to the ones obtained for the substituted porphyrin alone.[50]

3.4. Excited-State Structures. As mentioned previously, the broad and weak absorption band in the near-IR region of the $H_2P-O34-C_{60}$ absorption spectrum is attributed to the g-CTC absorption. The Franck−Condon state of g-CTC undergoes conformational relaxation toward the minimum of its PES (i.e., the ex-CT complex, see Figure 3). In general, the formation of ex-CTC is considered to have a strong impact on the dynamics of the ET. Thus, the theoretical investigation of the energy and geometric characteristics of ex-CTC are important in elucidating the mechanism and dynamics of ET. In addition, the reorganization energy λ accompanying the formation of ex-CTC from the locally excited singlet state of porphyrin $(H_2P-O34)^{1S}-C_{60}$ as defined in the Marcus theory of electron transfer[51] is an important quantity for calculating the rate constants of the ET.[3−8,10,15,17] Figure 3 presents a schematic representation drawn on the basis of the TD-DFT results for the PESs of the ground, ex-CTC, and $(H_2P-O34)^{1S}-C_{60}$ states.

The bullet points marked on the parabola representing the PES of the ground state are obtained from the ground-state geometry optimization of the dyad and by a single-point calculation on the structure of ex-CTC. In addition, several points on the line segment between the bullets are obtained as corresponding ground-state geometries of the excited-state structures during the TD-DFT optimization. The line segment between the bullets drawn on the parabola representing the PES of the ex-CT complex is obtained during the TD-DFT optimization. The optimization starts from the F−C state of the g-CT complex, for which the energy is determined by TD-DFT calculations with the ground-state optimized structure. The bullet points drawn on the parabola representing the PES of the locally excited porphyrin state are obtained from the TD-DFT calculations with the ground-state structures, without optimizing the $(H_2P-O34)^{1S}-C_{60}$ state.

To investigate the geometrical changes accompanying the relaxation of the Franck−Condon state of g-CTC (see Figure 3), we have performed two geometry optimizations[52] of the first excited singlet state of the dyad. The PBE and SVWN functionals have been used in the excited-state optimizations of the PBE and SVWN optimized ground-state geometries, respectively. The use of the B3LYP functional is not practical from a computational time point of view. The optimization of the excited-state geometry drives the cc distance from 7.1 to 7.4 Å with TD-DFT/PBE and from 6.3 to c.a. 6.5 Å with TD-DFT/SVWN. The increase in the donor−acceptor distance can be explained by a shift of the positions of the ground- and excited-state PES minima relative to each other. According to the results of the excited-state TD-DFT geometry optimizations of $H_2P-O34-C_{60}$, the relative shift of PESs is similar to that schematically drawn in Figure 3. Additional test calculations were performed with the SVWN functional, for which the computational labor is the smallest. The test calculations consist of the SVWN optimization of the first excited state of the dyad
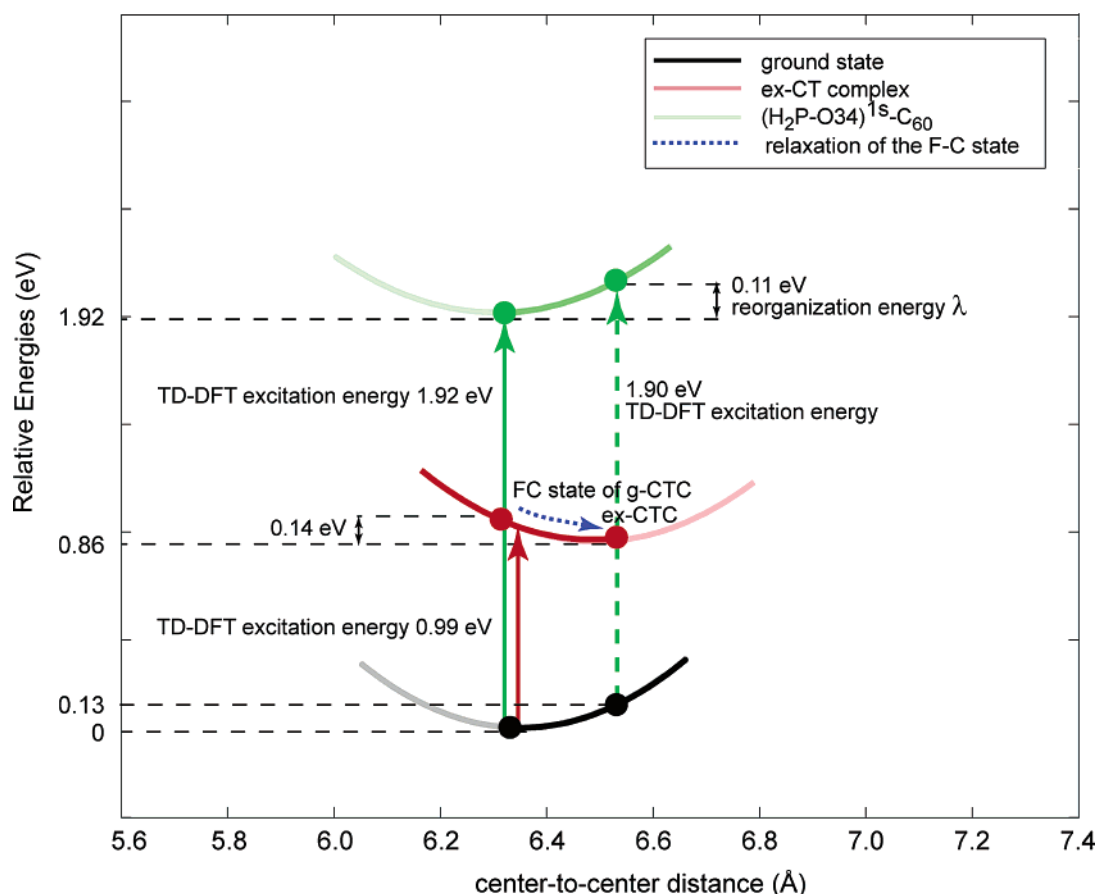
Figure 3. Schematic representations of the ground state and excited state (lowest and $(H_2P-O34)^{1s}-C_{60}$) potential energy curves drawn on the basis of the results obtained by TD-DFT calculations with the SVWN functional.

starting from the B3LYP optimized ground-state structure for which the cc distance is the largest out of the calculated ones (see Table 1). During the optimization, the cc distance decreases with the excited-state energy, thus supporting the schematic representation of Figure 3. Both the SVWN and the PBE excited-state optimizations predict that the relaxation of the excited state of g-CTC from its Franck−Condon state is accompanied by a decrease in the energy of approximately 0.14 eV.

The value of 0.11 eV for the reorganization energy λ is calculated by using (a) the results of the TD-DFT/SVWN calculations presented in section 3.3 and in Figure 3 for the transitions leading from the ground state of the dyad to the F−C state of g-CTC and to the $(H_2P-O34)^{1s}-C_{60}$ state, (b) the relaxation energy of the F−C state of g-CTC (see Figure 3), and (c) the TD-DFT excitation energy (1.90 eV) of the electronic transition from the ground-state structure corresponding to ex-CTC to the PES of the $(H_2P-O34)^{1s}-C_{60}$. If the solvent reorganization energy is considered negligible, as it is in principle in the case of ex-CTC in nonpolar solvents,[13] the calculated change in energy compares very well with the value of the total reorganization energy (0.11 eV) calculated from the experimental results.[3] However, if the total reorganization energy is split into solvent and internal reorganization energies[3,10] a value of 0.054 eV for the internal reorganization energy of the excited state of the dyad is obtained. In this case, the TD-DFT results yield a value that is more than twice as large as the one calculated from the experimental results.

The electric dipole moments of the excited state increase almost linearly during the optimization. The dipole moments of the optimized excited states are 25 and 18 D after the TD-

DFT optimizations employing PBE and SVWN, respectively. The values of the dipole moments in the excited state represent 60−70% of the dipole moment created by the transfer of one whole electron from the center of the porphyrin to the center of the fullerene. These values support the general description of the exciplex as having considerable CT character. Complete charge separation and formation of the CSS state are expected at large porphyrin−fullerene distances.

4. Conclusion

In this study, we have performed DFT and TD-DFT calculations using LDA, GGA, and hybrid functionals to investigate the structure, photoabsorption, and excited states of a covalently bonded porphyrin fullerene dyad $(H_2P-O34-C_{60})$ that exhibits computationally challenging ground-state and excited-state properties. Besides the characterization of the dyad, we were interested in analyzing the influence of the fullerene−porphyrin cc distance on the properties of the dyad. We also aimed at testing the performance of different functionals in describing (a) the CT character of the dyad in the ground state, (b) long-range CT excited states, and (c) the changes accompanying the relaxation of excited states.

The fullerene−porphyrin cc distance significantly affects several properties of the dyad, especially when porphyrin and fullerene are closely spaced as in the case of the SVWN optimized structure. The ground-state cc equilibrium distance between the donor and the acceptor moieties is 6.3, 7.1, and 7.9 Å with the SVWN, PBE, and B3LYP functionals, respectively. The associated charge transfer of 0.15, 0.11, and 0.09 electrons is shown to depend on this distance but not directly on the functional itself. The same trend is seen in the HOMO−

LUMO differences results and in the lowest excitation energies, except for the hybrid functional calculations in which case the functional has a significant influence. The PBE0 calculations yield the largest HOMO$-$LUMO gap and the highest energy for the lowest electronic excitation.

The TD-DFT optimization of the first excited state of $H_2P-O34-C_{60}$ offers both a qualitative and a quantitative picture of the ex-CTC formation process. The hybrid functional was not found to be practical for excited-state conformational relaxation with the present computing resources. With LDA, the relaxation increases the cc distance by about 0.2 Å, which is associated with a 0.14 eV decrease in energy. As compared to the ground-state dipole moment of about 4 D, the relaxed excited-state charge-transfer complex dipole moment turns out to become about 20 D, which corresponds to 0.60$-$0.70 electron.

The excitation that corresponds to the formation of a locally excited singlet porphyrin -state $(H_2P-O34)^{1S}-C_{60}$ is also considered. The excitation energy of about 2 eV depends little on the cc distance and on the functional. However, the number of electronic excitations calculated between the excitation of g-CTC and the first locally excited singlet porphyrin state depends largely on the functional that is used. The B3LYP functional yields the smallest number of excitations.

References and Notes

(1) Gust, D.; Moore, T. A.; Moore, A. L. *Acc. Chem. Res.* **1993**, *26*, 198.

(2) Guldi, D. M. *Chem. Soc. Rev.* **2002**, *31*, 22.

(3) Vehmanen, V.; Tkachenko, N. V.; Imahori, H.; Fukuzumi, S.; Lemmetyinen, H. *Spectrochim. Acta, Part A* **2001**, *57*, 2229.

(4) Tkachenko, N. V.; Rantala, L.; Tauber, A. Y.; Helaja, J.; P. Hynninen, H.; Lemmetyinen, H. *J. Am. Chem. Soc.* **1999**, *121*, 9378.

(5) Vehmanen, V.; Tkachenko, N. V.; Tauber, A. Y.; Hynninen, P.; Lemmetyinen, H. *Chem. Phys. Lett.* **2001**, *345*, 213.

(6) Kesti, T. J.; Tkachenko, N. V.; Vehmanen, V.; Yamada, H.; Imahori, H.; Fukuzumi, S.; Lemmetyinen, H. *J. Am. Chem. Soc.* **2002**, *124*, 8067.

(7) Vehmanen, V.; Tkachenko, N. V.; Efimov, A.; Damlin, P.; Ivaska, A.; Lemmetyinen, H. *J. Phys. Chem. A* **2002**, *106*, 8029.

(8) Tkachenko, N. V.; Lemmetyinen, H.; Sonoda, J.; Ohkubo, K.; Sato, T.; Imahori, H.; Fukuzumi, S. *J. Phys. Chem. A* **2003**, *107*, 8834.

(9) Imahori, H.; Tkachenko, N. V.; Vehmanen, V.; Tamaki, K.; Lemmetyinen, H.; Sakata, Y.; Fukuzumi, S. *J. Phys. Chem. A* **2001**, *105*, 1750.

(10) Vehmanen, V.; Ph.D. Thesis, Tampere University of Technology, Tampere, Finland, November 2002.

(11) Tappura, K.; Cramariuc, O.; Hukka, T. I.; Rantala, T. T. *Phys. Chem. Chem. Phys.* **2005**, *7*, 3126.

(12) Mataga, N.; Chosrowjan, H.; Taniguchi, S. *J. Photchem. Photobiol., C* **2005**, *6*, 37.

(13) Waluk, J., Ed. *Conformational Analysis of Molecules in Excited States*; Wiley-VCH: Weinheim, 2000; Ch. 4.

(14) Luo, C.; Guldi, D. M.; Imahori, H.; Tamaki, K.; Sakata, Y. *J. Am. Chem. Soc.* **2000**, *122*, 6535.

(15) Chukharev, V.; Tkachenko, N. V.; Efimov, A.; Guldi, D. M.; Hirsch, A.; Scheloske, M.; Lemmetyinen, H. *J. Phys. Chem. B* **2004**, *108*, 16377.

(16) Schuster, D. I.; Cheng, P.; Jarowski, P. D.; Guldi, D. M.; Luo, C.; Echegoyen, L.; Pyo, S.; Holzwarth, A. R.; Braslavsky, S. E.; Williams, R. M.; Klihm, G. *J. Am. Chem. Soc.* **2004**, *126*, 7257.

(17) Kesti, T.; Ph.D. Thesis, Tampere University of Technology, Tampere, Finland, December 2002.

(18) Ruiz, E.; Salahub, D. R.; Vela, A. *J. Phys. Chem.* **1996**, *100*, 12265.

(19) Phillips, J. A.; Cramer, C. J. *J. Chem. Theory Comput.* **2005**, *1*, 827.

(20) Casida, M. *Recent Advances in Density Functional Methods*; Chong, D. P., Ed.; World Scientific: Singapore, 1995; Vol. 1.

(21) Casida, M. *Recent Developments and Applications of Modern Density Functional Theory*; Seminario, J. M., Ed.; Elsevier: Amsterdam, 1996.

(22) Petersilka, M.; Gossmann, U. J.; Gross, E. K. U. *Phys. Rev. Lett.* **1996**, *76*, 1212.

(23) Petersilka, M.; Gross, E. K. U. *Int. J. Quantum Chem.* **1996**, *30*, 181.

(24) Jamorski, C.; Casida, M.; Salahub, D. R. *J. Chem. Phys.* **1996**, *104*, 5134.

(25) Bauernschmitt, R.; Ahlrichs, R. *Chem. Phys. Lett.* **1996**, *256*, 454.

(26) Stratmann, R. R.; Scuseria, G. E.; Frisch, M. J. *J. Chem. Phys.* **1998**, *109*, 8218.

(27) Bauernschmitt, R.; Ahlrichs, R.; Hennrich, F. H.; Kappes, M. M. *J. Am. Chem. Soc.* **1998**, *120*, 5052.

(28) van Gisberg, S. J. A.; Rosa, A.; Ricciardi, G.; Baerends, E. J. *J. Chem. Phys.* **1999**, *111*, 2499.

(29) Ricciardi, G.; Rosa, A.; van Gisbergen, S. J. A.; Baerends, E. J. *J. Phys. Chem. A* **2000**, *104*, 635.

(30) Dreuw, A.; Head-Gordon, M. *J. Am. Chem. Soc.* **2004**, *126*, 4007.

(31) Tozer, D. J.; Amos, R. D.; Handy, N. C.; Roos, B. J.; Serrano-Andres, L. *Mol. Phys.* **1999**, *97*, 859.

(32) Sobolewski, A. L.; Domcke, W. *Chem. Phys.* **2003**, *294*, 73.

(33) Toivonen, T. L. J.; Hukka, T. I.; Cramariuc, O.; Rantala, T. T.; Lemmetyinen, H. *J. Phys. Chem. A*, accepted.

(34) Slater, J. C. *Quantum Theory of Molecules and Solids*; McGraw-Hill: New York, 1974; Vol. 4.

(35) Vosko, S. H.; Wilk, L.; Nusair, M. *Can. J. Phys.* **1980**, *58*, 1200.

(36) Dirac, P. A. M. *Proc. R. Soc. London* **1929**, *123*, 714.

(37) Slater, J. C. *Phys. Rev.* **1951**, *81*, 385.

(38) Perdew, J. P.; Chevary, J. A.; Vosko, S. H.; Jackson, K. A.; Pederson, M. R.; Singh, D. J.; Fiolhais, C. C. *Phys. Rev. B* **1992**, *46*, 6671.

(39) Perdew, J. P.; Burke, K.; Ernzerhof, M. *Phys. Rev. Lett.* **1996**, *77*, 3865.

(40) Lee, C.; Yang, W.; Parr, R. G. *Phys. Rev. B* **1988**, *37*, 785.

(41) Becke, A. D. *J. Chem. Phys.* **1993**, *98*, 5648.

(42) Perdew, J. P.; Ernzerhof, M.; Burke, K. *J. Chem. Phys.* **1996**, *105*, 9982.

(43) Schäfer, A.; Horn, H.; Ahlrichs, R. *J. Chem. Phys.* **1992**, *97*, 2571.

(44) Dunning, T. H., Jr. *Chem. Phys.* **1989**, *90*, 1007.

(45) Eichkorn, K.; Treutler, O.; Öhm, H.; Häser, M.; Ahlrichs, R. *Chem. Phys. Lett.* **1995**, *240*, 283.

(46) Ahlrichs, R.; Bär, M.; Häser, M.; Kälmel, C. *Chem. Phys. Lett.* **1989**, *162*, 165.

(47) Scheidt, W. R.; Lee, Y. J. *Struct. Bonding (Berlin)* **1987**, *64*, 1.

(48) Parusel, A. B. J. *J. Photochem. Photobiol., B* **2000**, *55*, 188.

(49) Mengtao, S.; Chen, Y.; Song, P.; Ma, F. *Chem. Phys. Lett.* **2005**, *413*, 94.

(50) Cramariuc, O.; Hukka, T. I.; Rantala, T. T. *J. Phys. Chem. A* **2004**, *108*, 9441.

(51) Marcus, R. A. *Annu. Rev. Phys. Chem.* **1964**, *15*, 155.

(52) Furche, F.; Ahlrichs, R. *J. Chem. Phys.* **2002**, *117*, 7433.